Proc. of the 2018 International Symposium on Electromagnetic Compatibility (EMC Europe 2018), Amsterdam, The Netherlands, August 27−30, 2018.

Development and Applications of a Fiber-Coupled Atom-Based Electric Field Probe

Christopher L. Holloway, Matt T. Simons, Marc Kautz, Perry F. Wilson, and Joshua A. Gordon

National Institute of Standards and Technology (NIST)
325 Broadway, Boulder, CO 80305, USA
holloway@boulder.nist.gov

***Abstract*—We are developing a fundamentally new atom-based approach for electric (E) field measurements. This new approach will lead to a self-calibrated, SI traceable, E-field measurement, providing us with the capability to perform measurements on a fine spatial resolution in both the far- and near-fields. Here, we discuss the development and applications of the first moveable fiber-coupled version of this atom-based E-field measurement approach. We show results for various measurements including: far-field measurements of the E-fields, measurements of the E-field distribution along the surface of a circuit board, field measurements in apertures, measurements of the directivity pattern of a horn antenna, and measurements made in a GTEM cell.**

I. Introduction

Significant progress has recently been made in the development of a novel Rydberg-atom spectroscopic approach for radio-frequency (RF) electric (E) field strength measurements [1]-[9]. This approach utilizes the phenomena of electromagnetically induced transparency (EIT) and Autler-Townes (AT) splitting [1]-[10], and leads to a direct International System of Units (SI) traceable, self-calibrated measurement.

While various international metrology organizations around the world are beginning to investigate this new approach as a possible new standard for E-field measurements and calibrations, all previous investigations and measurements have been confined to an optical table. This confinement is a result of the fact that this technique requires the two lasers (probe and coupling lasers) to overlap inside the vapor cell. In order to overcome these issues, we have developed the first fiber-coupled vapor cell (see Fig. 1) [11], where the two counter propagating lasers are carefully overlapped inside the vapor cell while it is moved off the optical table. Moving the probe off of the optical table allows measurements to be performed in free space and in other standard RF metrology environments. The new probe consists of a 10-mm cubic vapor cell (made with all dielectric material, i.e., glass) filled with cesium ^{133}Cs and two optical fibers with lenses attached with UV curing epoxy at either end (see Fig. 1). We have performed various measurements in order to illustrate the new probe's capabilities. These experiments are described in this paper.

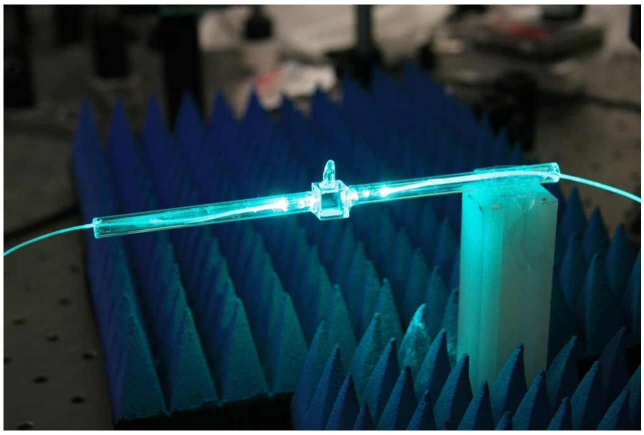

Fig. 1: Fiber-coupled atom-based E-field probe.

II. Description of the Atom-Based Approach

The measurement approach uses a vapor of alkali atoms (placed in a glass cell, referred to as a "vapor- cell") as the active medium for the radio frequency (RF) E-field measurement. The basic concept is that by manipulating alkali atoms with both optical (laser) fields and RF fields, it is possible to cause a laser to transmit through the vapor cell where it would normally be absorbed by the atoms in the vapor cell. Rubidium (^{85}Rb) and cesium (^{133}Cs) are the two atomic species that are typically used in the approach. A typical measurement setup is shown in Fig. 2(a). This measurement approach can be represented by the four-level atomic system shown in Fig. 2(b), see [1]-[3] and [9] for details.

A "probe" laser is used to probe the response of the ground-state transition of the atoms and a second laser ("coupling" laser) is used to excite the atoms to a Rydberg state. In the presence of the coupling laser, a destructive quantum interference occurs and the atoms become transparent to the resonant probe laser. This is the concept of EIT, in which a transparency window is opened for the probe laser light, and the probe light transmission is increased. The coupling laser wavelength is chosen such that the atoms are in a sufficiently high state (a Rydberg state) so that a RF field coherently couples two Rydberg states (levels 3 and 4 in Fig. 2(b)). The RF field in the four-level atomic system causes constructive interference of excitation pathways within the EIT transmission window, resulting in a decreased transmission of the probe laser and AT splitting of the EIT peak.

A typical power measurement from the detector when the laser is scanned across this wavelength is shown Fig. 3(a) (where $\Delta_p=\omega_p-\omega_o$, ω_o is the on-resonance angular frequency of the ground state transition and ω_p is the angular frequency of the probe laser). The bottom curve shows the measured probe laser spectrum with no coupling laser, the top curve is the spectrum with the coupling and no RF, and the middle curves is the spectrum with both the coupling laser and with RF on (note the wings of all three curves normally would lay on top of one another, but they are shifted here for ease of viewing). For the top curve, notice at Δ_p=0, the power on the detector is larger than the Doppler background, i.e., the global inverted bell-shaped behavior.

The wavelength of the coupling laser is chosen judiciously such that the atoms are excited to a very high energy, where an RF source is at a resonant frequency that causes an atomic transition to a nearby state (i.e., an RF atomic transition). When the RF source is turned on, the EIT signal splits into two (this splitting is called Autler-Townes (AT) splitting), see the middle curve in Fig. 3(a). To increase the EIT signal-to-noise, we modulate the coupling-laser amplitude with a 50/50 duty-cycle 30 kHz square wave and detect any resulting modulation of the probe transmission with a lock-in amplifier. This removes the Doppler background and isolates the EIT signal. Fig. 3(b) shows a typical EIT signal from the lock-in amplifier for different values of RF field levels. The splitting of the EIT peak is indicated by Δf_m.

(a) Experimental setup.

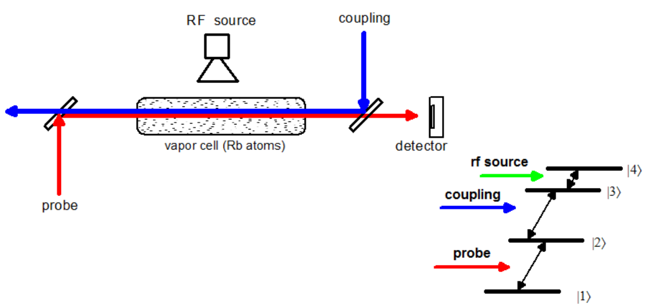

(b) Vapor-cell and four-level system.

Fig. 2: Measurement setup and four-level atomic system.

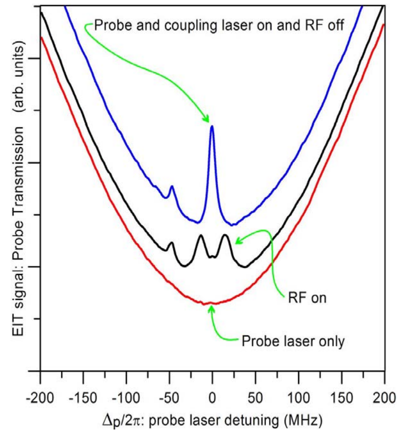

(a) EIT signal without lock-in.

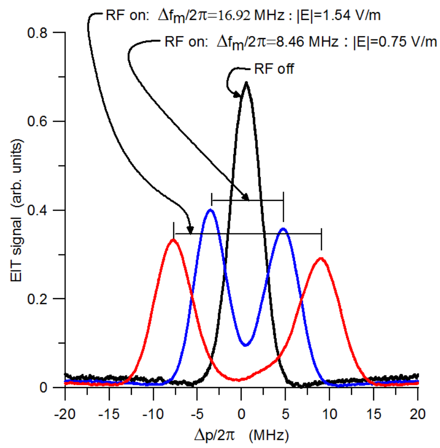

(b) EIT signal with lock-in.

Fig. 3: Typical measurement of the EIT signal.

This splitting (Δf_m) of the probe laser spectrum is easily measured and is directly proportional to the applied RF E-field amplitude. Once this Δf_m is measured, the RF E-field strength is obtained from [1]-[3] and [9]:

$$|E| = 2\pi \frac{\hbar}{\wp} \frac{\lambda_p}{\lambda_c} \Delta f_m \quad , \tag{1}$$

where $\hbar$ is Planck's constant, $\wp$ is the atomic dipole moment of the RF atomic transition, and λ_p and λ_c are the wavelengths of the probe and coupling lasers, respectively. The ratio λ_p/λ_c accounts for the Doppler mismatch of the probe and coupling lasers [10], assuming the probe and coupling lasers are counter-propagating in the cell. One can also scan the coupling laser and not the probe laser during the experiments. If the coupling laser is scanned, it is not required to correct for the Doppler mismatch, and λ_p/λ_c ratio is not needed, see [9] for details. The measurement based on (1) is a direct SI-traceable measurement, in that it is directly related to Planck's constant. To estimate $|E|$, Δf_m is obtained from a measurement, Planck's constant is known, and $\wp$ is calculated from first principles (see [3] for discussion on determining $\wp$).

One of the advantages of this new approach is that it is very broadband. In fact, utilizing the experiment setup shown in Fig. 2(a), we can measure the E-field strength over a frequency range from hundreds of MHz to 1 THz. Fig. 4 shows measurements for six different frequencies ranging from 9.22 GHz to 182 GHz using two different atomic species (^{85}Rb and ^{133}Cs). In this figure, we also compare the estimated E-field obtained for this atom-based approach to both far-field calculations and to numerical simulations. We see that the atom-based approach correlates very well with both (uncertainties are discussed below).

III. Fiber-Coupled E-Field Probe

Most experiments using this atom-based approach have been confined to an optical table, see Fig. 2(a). For the technique to be useful, the probe needs to be moved off the table and constructed such that it can be moveable. Toward this goal, we have developed the first fiber-coupled vapor-cell E-field probe (see Fig. 1). We have used this probe in various experiments, which are discussed next.

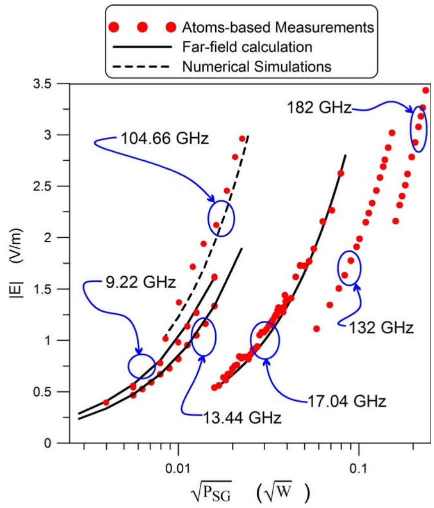

Fig. 4: A comparison of the measured E-field to results obtained from far-field calculations and from a full-wave numerical simulation.

A. Mapping the Fields In a GTEM Cell

We used the fiber-probe to measure the E-field inside a gigahertz transverse electromagnetic (GTEM) cell. This allows us to access the field variability along the longitudinal axis as a function of frequency. The fiber probe was placed at the center of a GTEM cell and moved to different locations along the longitudinal axis, see Fig. 5. In these experiments, we measured the E-field at three different positions in the GTEM cell at three different frequencies. Fig. 6 shows the measured results for the total field. For reference, we also shown results for the calculated field inside the GTEM, see eq. (E.2) in [12]. From these experiments, we see that E-field varies as a function of frequency and position, due to impedance variations and higher-order modes. The high frequency variation with frequency is also shown in [13]. Notice that the variability becomes worst the furthest from the input of the GTEM feed, as expected.

Fig. 5: Fiber-probe inside a GTEM cell.

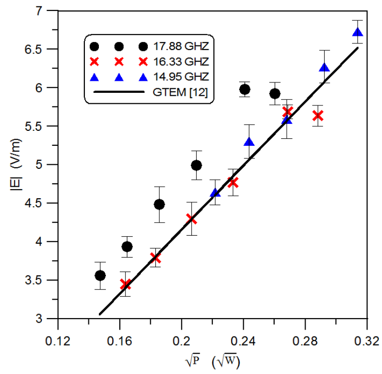

(a) 2.64-m from input.

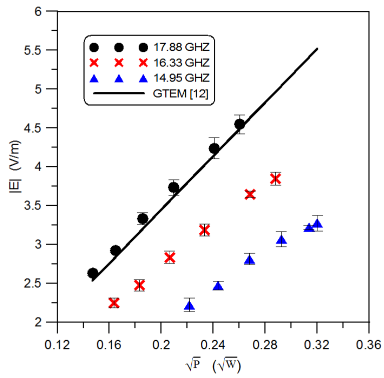

(b) 3.08-m from input.

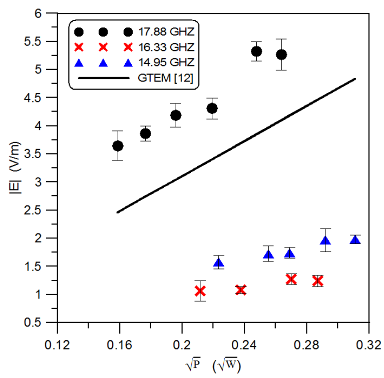

(c) 3.49-m from input.

Fig. 6: E-field mapping inside a GTEM cell.

B. Imaging the Fields Above a CPW Line

In order to illustrate the near-field imaging capability of the fiber-coupled probe, we imaged the total E-field at various heights (*h*) across the surface of a co-planar waveguide (CPW) line, see Fig. 7. The CPW has a center strip of 3 mm, gaps of 2 mm, and a substrate ($\varepsilon = 3.5$) of thickness 1.52 mm. Fig. 8 shows the scans at six different heights for a frequency of 11.6 GHz. In order to show the repeatability of this probe we performed three sets of measurements for each height and the error-bars represent all these measurements. As a check, we show results obtained from HFSS (mentioning this full-wave simulator does not imply an endorsement, but serves to clarify the numerical program used) for h = 6.64 mm. While the HFSS simulations have the same general behavior as the measured results, the differences are due to the fact the that the HFSS results are for an infinitely wide ground plane CPW. These results show the probe capability for near-field imaging and field-mapping across the surface of printed-circuit board structures, which will be used in the future to support calibrated on-wafer measurements of high-speed (high-frequency) integrated circuits. The fiber-coupled probe allows for much finer spatial resolution than is possible with current E-field probes. The spatial resolution is 70 μm, which is essentially the width of the laser beams [1].

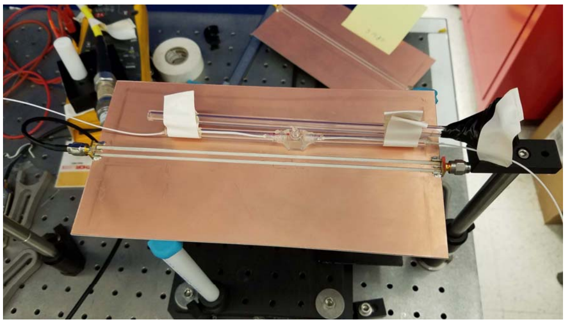

Fig. 7: Fiber-probe above a CPW line.

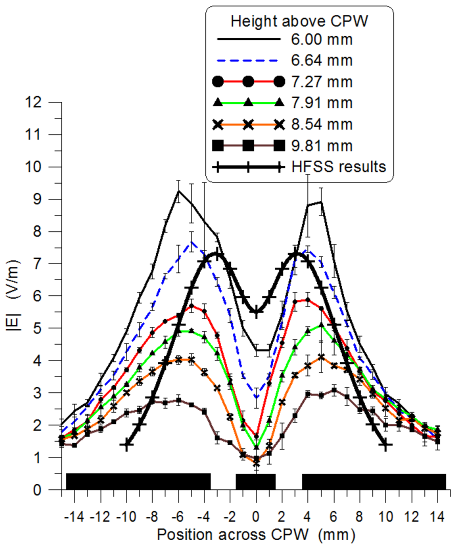

Fig. 8: Measured E-field above a CPW line.

C. Antenna Pattern Measurements

We used the fiber-coupled probe to measure the antenna pattern of a Narda 640 standard gain horn antenna (mentioning this product does not imply an endorsement, but serves to clarify the antenna used). The experimental setup for these measurements is shown in Fig. 9. In these measurements, the fiber-coupled probe was placed 0.835 m from the horn antenna (in the quasi-far-field). During the experiments, we scanned the antenna from bore site to an angle of 60^{o}. We scanned both the E-plane and H-plane of the horn antenna and the total E-field was measured. Fig. 10 shows the measured antenna patterns for both the E-plane and H-plane at 11.6 GHz. Also shown in this figure are results obtained in an anechoic chamber test range [14] at 9.4 GHz. Good correlation between the two types of measurements is seen. The deviations are because our measurements were performed in a laboratory with no RF absorber on the walls and the laboratory had several objects in the room, see Fig. 9. Thus, our results suffer from some background scattering.

D. Imaging the Fields In an Aperture

As another mapping example, we performed measurements across an aperture located on the side of a small transverse electromagnetic (TEM) cell, see Fig. 11. The TEM cell size was 5.5 cm wide, 2.7 cm tall, with a circular aperture of radius 0.75 cm. The fiber-coupled probe was scanned across the aperture for a given input power to the TEM cell. We performed measurements of the total field at the aperture 6 mm from the aperture at 21.6 GHz and 29.5 GHz. These data are shown in Fig. 12. Since the TEM cell is highly multi-moded at these two frequencies and the aperture fields cannot readily be calculated, and measurements are the best approach to determine the near-fields. The fiber-probe allows for such a measurement.

IV. UNCERTAINTIES

Understanding the uncertainties of this technique is an important step if this method is to be accepted as a standard calibration technique. The various aspects that contribute to the uncertainties of this technique are currently being investigated and are summarized in [1]-[6], [9], and [15]. While the uncertainty analysis is still being performed, initial results indicate the uncertainties have the possibility of being below 0.1 -to- 0.5 dB.

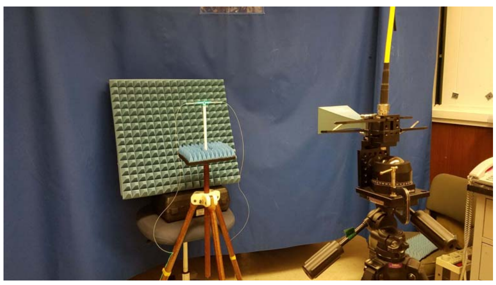

Fig. 9: Setup for the antenna pattern measurements.

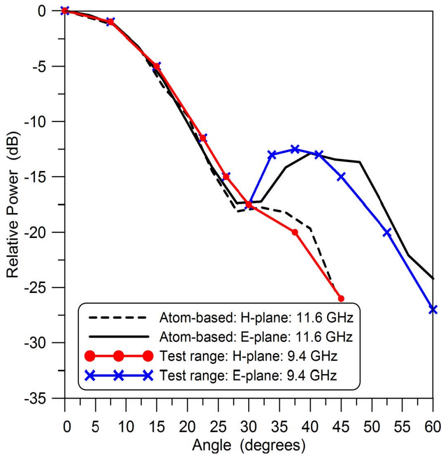

Fig. 10: Measured antenna pattern.

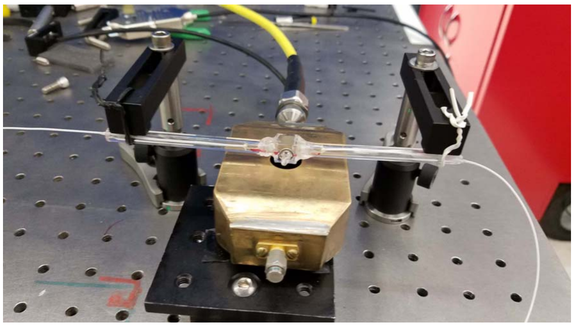

Fig. 11: Fiber-probe at aperture of small TEM cell.

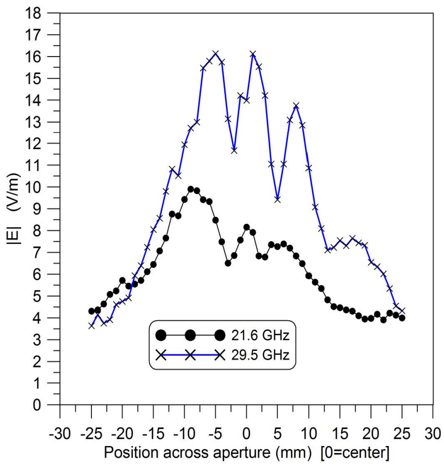

Fig. 12: Measured E-field across the aperture at a height of 6 mm for two different frequencies.

V. Summary

In this paper, we discussed the development of a fundamentally new approach for a SI traceable E-field measurement. We have shown the evolution of this technique from being confined to an optics table to the first fiber-coupled atom-based E-field probe. We illustrate the utility of this probe by showing results for fields inside a GTEM, near-field imaging of printed circuit boards and apertures, and antenna pattern measurements. While there is still a lot of work to be done in order for this technique to accepted as a new E-field standard, these results in this paper are useful steps toward making this probe a practical device.

References

[1] C.L. Holloway, M.T. Simons, J.A. Gordon, P.F. Wilson, C.M. Cooke, D.A. Anderson, and G. Raithel, "Atom-Based RF Electric Field Metrology: From Self-Calibrated Measurements to Sub-Wavelength and Near-Field Imaging", *IEEE Trans. on Electromagnetic Compat.,* vol. 59, no. 2, 717-728, 2017.

[2] J.A. Sedlacek, A. Schwettmann, H. Kubler, R. Low, T. Pfau and J.P. Shaffer, "Microwave electrometry with Rydberg atoms in a vapour cell using bright atomic resonances", *Nature Phys.,* vol. 8, 819, 2012.

[3] C.L. Holloway, J.A. Gordon, A. Schwarzkopf, D.A. Anderson, S.A. Miller, N. Thaicharoen, and G. Raithel, "Broadband Rydberg Atom-Based Electric-Field Probe for SI-Traceable, Self-Calibrated Measurements," *IEEE Trans. on Antenna and Propag.* vol. 62, no. 12, 6169-6182, 2014.

[4] H. Fan, S. Kumar, J. Sedlacek, H. Kubler, S. Karimkashi, and J.P. Shaffer, "Atom based RF electric field sensing," *J. of Phys. B: Atomic, Molecular and Optical Physics*, vol. 48, 202001, 2015.

[5] H. Fan, S. Kumar, J. Sheng, J.P. Shaffer, C.L. Holloway and J.A. Gordon, "Effect of Vapor Cell Geometry on Rydberg Atom-based Radio-frequency Electric Field Measurements", *Physical Review Applied*, vol. 4, 044015, November, 2015.

[6] C.L. Holloway, J.A. Gordon, M.T. Simons, H. Fan, S. Kumar, J.P. Shaffer, D.A. Anderson, A. Schwarzkopf, S. A. Miller, N. Thaicharoen, and G. Raithel, "Atom-based RF electric field measurements: an initial investigation of the measurement uncertainties," *Joint IEEE Intern. Symp. on EM and EMC Europe*, Dresden, Germany, pp. 467-472, Aug. 2015.

[7] D.A. Anderson, S.A. Miller, G. Raithel, J.A. Gordon, M.L. Butler, and C.L. Holloway, *Physical Review Applied*, vol. 5, 034003, 2016.

[8] D.A. Anderson, S.A. Miller, A. Schwarzkopf, C.L. Holloway, J.A. Gordon, N. Thaicharoen, and G. Raithelet, *Physical Review A*, vol. 90, 043419, 2014.

[9] C.L. Holloway, M.A. Simons, J.A. Gordon, A. Dienstfrey, D.A. Anderson, and G. Raithel, "Electric Field Metrology for SI Traceability: Systematic Measurement Uncertainties in Electromagnetically Induced Transparency in Atomic Vapor", *J. of Applied Physics*, vol. 121, 233106, 2017.

[10] A.K. Mohapatra, T.R. Jackson, and C.S. Adams, "Coherent optical detection of highly excited Rydberg states using electromagnetically induced transparency," *Phys. Rev. Lett.*, vol. 98, 113003, 2007.

[11] M.T. Simons, J.A. Gordon, and C.L. Holloway, "Fiber-coupled Vapor Cell for a Rydberg Atom-based RF Electric Field Sensor," submitted to *Applied Optics*, 2018.

[12] ICE 61000-4-20: Testing and measurement techniques Emission and immunity testing in transverse electromagnetic (TEM) waveguides.

[13] P.F. Wilson, "Higher-order mode fields distribution in asymmetric transverse electromagnetic cells, *Radio Science*, vol. 26, no. 2, 551-557, 1991.

[14] T.J. Duck, B. Firanski, F.D. Lind, and D. Sipler, "Aircraft-protection radar for use with atmospheric lidars", *Applied Optics*, vol. 44, no. 23, pp. 4937-4945, 2005.

[15] M.T. Simons, M. Kautz, J. Gordon, and C.L. Holloway, "Uncertainties in Rydberg Atom-based RF E-field Measurements*", EMC Europe 2018*, Amsterdam, NL, Aug. 27-30, 2018